

Circular dichroism simulations of chiral buckybowls by means curvature analyses

Giovanni Bella^{*}, Giuseppe Bruno, Antonio Santoro^{*}

Department of Chemical, Biological, Pharmaceutical and Environmental Sciences, University of Messina, Viale F. Stagno d'Alcontres 31, Messina 98166, Italy

ARTICLE INFO

Keywords:

Buckybowl
Chirality
Curvature
TD-DFT
Circular dichroism

ABSTRACT

A detailed understanding and interpretation of chiral properties of molecular systems, especially in condensed phase, often requires computational models that allow their structural and electronic features to be connected to the observed experimental spectra. The present paper is focused on modelling the circular dichroism spectra of chiral *buckybowls*, combining topological aspects and the density functional theory. For the first time Ball Pivoting Algorithm was proposed to hook up the chemical topology to the DFT through the surface reconstruction. Particularly, the gaussian curvature of a constructed probe set of corannulene and sumanene derivatives was used as discriminant parameter to benchmark a list of 10 functionals (B3LYP, B97D, M06-2X, HSEH1PBE, wB97XD, CAM-B3LYP, LC-wPBE, TPSSPTSS, mPW1PW91 and APFD). The latter provide to be noticeably accurate to reproduce the curvature effect of the considered molecules. A TD-DFT/BOMD mixed approach provided a comprehensive overview of the spectral chiral pattern prediction trends when multiple DFT functionals are scanned. The preliminary topological analysis efforts were then recompensed with the very precise computed CD spectra, again APFD confirmed as the leader functional, this time for TD-DFT vertical transition calculations. Therefore, we strongly recommend the use of the of dispersion embedded APFD functional coupled with the 6-311++G(2d,2p) basis set for the computation of the functionalized chiral buckybowls ECD spectra.

© 2017 Elsevier Inc. All rights reserved.

Introduction

Carbon is probably the most versatile element in the periodic table in terms of its unrivalled ability to form a large number of allotropes [1]. *De facto*, there is a virtual alphabet of possible structures made exclusively of sp^3 - and sp^2 - hybridised carbon atoms, in these terms the absolutely well-known archetypal examples are diamond and graphene [2]. Focusing on sp^2 - carbon allotropes, it is possible to find exotic surface topologies by means bending or spherifying a single sheet of graphene, obtaining three-dimensional hexagonal lattice composed of fused benzenoid rings such as nanotubes, fullerenes and their derivatives [3]. Recently, a number C_{60} and C_{70} subunits have emerged in a variety of concave/convex fragments named buckybowls which can be considered as a polar cap of fullerene [4]. Within this premise, corannulene and sumanene undoubtedly occupy a venerated position among the nonplanar polycyclic aromatic compounds (Fig. 1).

Their characteristic bowl-shaped surfaces are caused by incorporation of five-membered rings into a sheet of benzenoids, consistent with Euler's rule [5], these geodesic polyarenes are considered to have

positive Gaussian curvature [6]. In positively curved systems the fusion pattern becomes crucial to obtain unique inherent chirality, so-called bowl chirality for convenience, basically this kind of asymmetry is reached in four cases (Fig. 2). 1) The π -extended buckybowl structure itself owns the chirality, i.e. hemifullerene (Fig. 2A); 2) Introducing one or more substituents on the rim of the bowl, i.e. trimethylsumanene (Fig. 2B), trimethylsumanenetrione; 3) Embedding heteroatoms into the conjugated carbon skeleton, i.e. triazasumanene (Fig. 2C); 4) A combination of the previous ones i.e. trithiomethyltriazasumanene (Fig. 2D).

Beyond the fascinating and complex stereodescriptor systems [7], the main obstacle to experimentally investigate the bowl chirality is the bowl inversion energy barrier that regulates the racemization process [8]. In this framework, despite the synthetic difficulties, many efforts were made to access to high bowl inversion barrier buckybowls [9–11]. When the flipping of curvature is thermally blocked an interesting chiroptical behaviour appears, leading to the different absorption of left- and right-handed circularly polarization light and exhibiting an opposite Cotton effect. Until now, a limited series of chiral buckybowls enantioselective resolved possessing stable CD spectra is present in literature

^{*} Corresponding authors.

E-mail addresses: gbella@unime.it (G. Bella), antonio.santoro@unime.it (A. Santoro).

<https://doi.org/10.1016/j.flatc.2023.100509>

Received 28 March 2023; Received in revised form 3 May 2023; Accepted 15 May 2023

Available online 23 May 2023

2452-2627/© 2023 The Authors. Published by Elsevier B.V. This is an open access article under the CC BY license (<http://creativecommons.org/licenses/by/4.0/>).

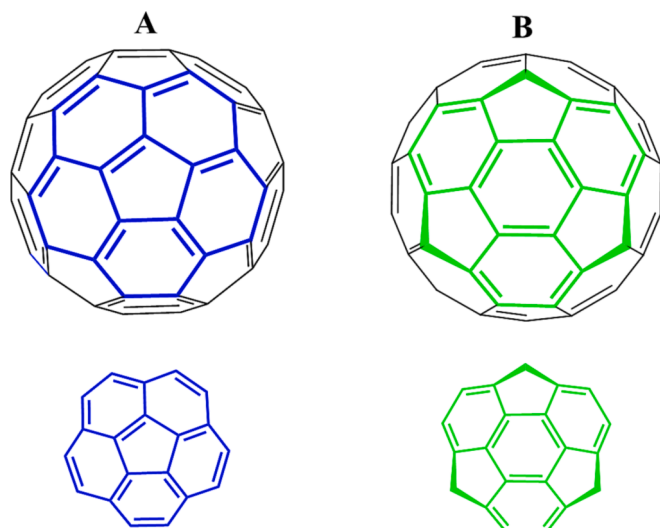


Fig. 1. (A) Corannulene ($C_{20}H_{10}$) subunit. (B) Sumanene ($C_{21}H_{12}$) subunit.

[12], (it should be noted that buckybowls, as common molecules, can also include structures with substituents bearing stereogenic carbons [13,14]). In this regard, due to the multiplicity and complexity of the factors coacting in determining the spectral frame, the interpretation of spectroscopic data based on experimental measurements alone can lead to uncertainties and ambiguities. On the following this ground, theoretical calculations turn into a powerful tool for analysing the connection between structure and spectroscopic diagnostic signals both for chiroptical and not-chiroptical spectroscopic techniques [15–17]. To accomplish this task, time-dependent density functional theory (TD-DFT) can guide the rational elucidation of complex CD spectra by providing insight in the chirality of the ground state, although such theoretical works based on buckybowls result still rare in the literatures [18]. In this article we propose a new approach to model the topologies of positively curved aromatic compounds through the atom by atom gaussian curvature in order to capture the compelling relationship between the molecules curvature and the absorption of circularly polarized light. At this point, it is useful to precise that our *modus operandi* will divide the manuscript into four levels: 1) Reconstruction of molecular surfaces starting from their atomic cartesian coordinate. 2) Calculation of local gaussian curvature for each atom belonging to the buckybowl skeleton. 3) Benchmark of functionals to choose the best level of theory to predict a reliable molecular curvature. 4) Reproduction of CD spectral shapes exploiting the selected configurations retrieved from Born-Oppenheimer molecular dynamics trajectories. For our goals, a

heterogeneous set enclosing five representative chiral buckybowls was drafted, for technical necessity just x-ray collected structures were contemplated and the bowl chirality was privileged, compound 2 was inserted because it is a *unicum* since it brings a stereogenic carbon on the hub (Fig. 3.).

Results and discussion

Surface reconstruction

Since the time of birth of chemistry, chemists are used to thinking about molecules as geometric entities in which atoms have a certain spatial arrangement. In the last century the introduction of new physical theories has revealed difficulties in bringing the concept of molecular geometry in harmony with the basic principles of quantum theory [19]. The drawback of the geometric approach is that the geometric parameters provide a local characterization of the molecule (i.e. they establish relations between two, three or four atoms) but certain spatial relations in molecules depend on the molecular architecture as a whole. In these cases, we should not focus on bond lengths and angles but rather the embedding of the molecule as a whole in three-dimensional space. Instead of conventional geometric structures (which are sets of atoms in the two- or three-dimensional space, whose distances are determined by the Euclidean metric), modern topology investigates sets with much more general properties. Changes in the molecular geometry, caused by intramolecular motions or by any kind of external influence (i.e. light absorption), but in which no chemical bond has been broken or formed, are therefore called *topological properties*. With this in mind, in order to evaluate a topological concept like curvature it is necessary to have a surface, and strictly speaking a molecule is more like a graph. Nevertheless, curved platforms like buckybowls offer the possibility to mathematically transform a point cloud into a surface. To date, there is no a standard method to convert a set of 3D points given by atomic coordinates into a single mesh, indeed there is large space of interpretation for connecting molecules with mathematics. Considering the lack of bibliographic proliferation in this regard, for our purposes we decided to adopt the Ball Pivoting Algorithm [20] (BPA) for finding a triangle mesh that interpolates a chemically organized set of points. This heuristic process can be traced back to the Delaunay triangulation, and it is abridged as follow: let the manifold M be the surface of a three-dimensional object embedded in \mathbb{R}^3 and P a sampling point set included in M , a φ -ball (where φ is the radius) can now lie on M without “falling” between sample points (P should be dense enough). The algorithm starts by locating a φ -ball in contact with three sample points (η_i, η_j, η_k) generating a seed triangle (green point in the third image of A series, Fig. 4), now we proceed by rotating the ball of radius φ from its initial position maintaining the contact with two initial points (i.e. two

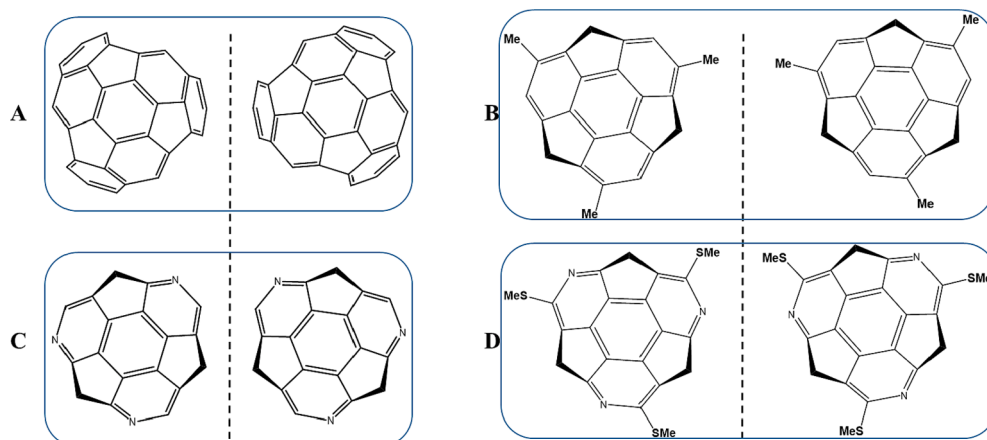


Fig. 2. Classification of chiral buckybowl derivatives: (A) Hemifullerene. (B) Trimethylsumanene. (C) Triazasumanene. (D) Trithiomethyltriazasumanene.

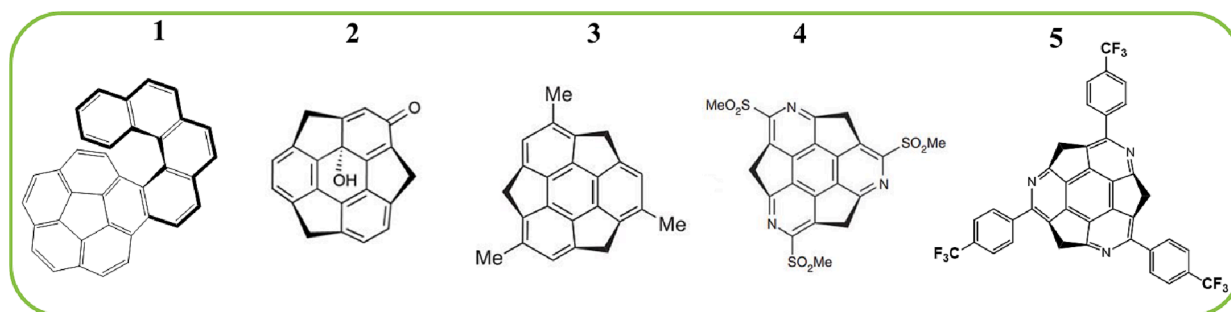


Fig. 3. Corannulene, sumanone, sumanene and triazasumanene units currently in our computational set.

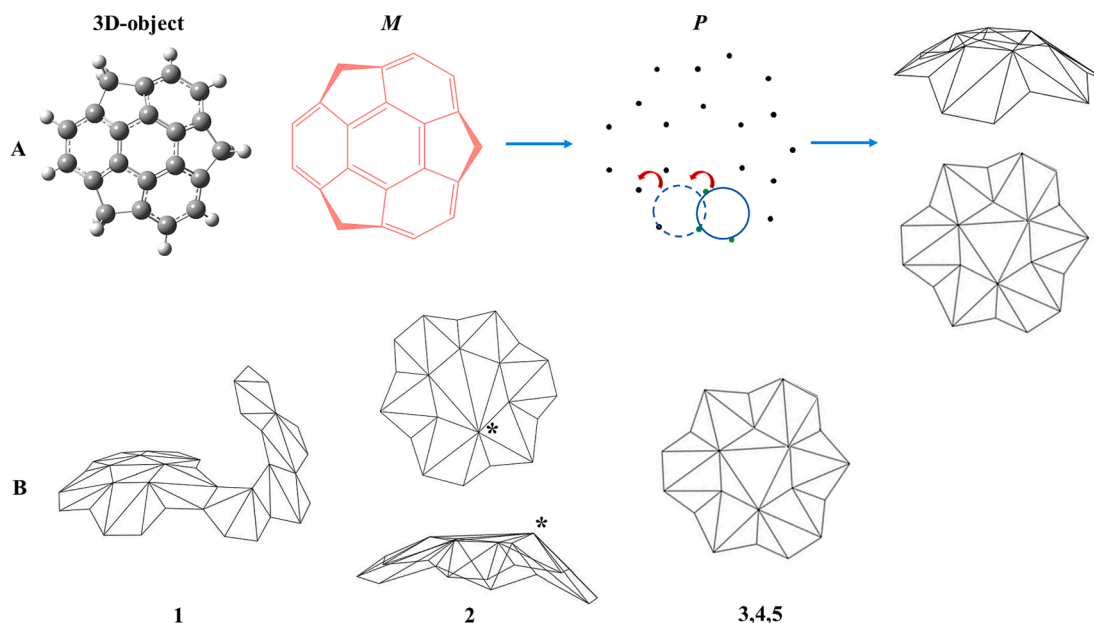


Fig. 4. (A) Ball pivoting algorithm to compute triangulated meshes. (B) Constructed surfaces of our target compounds in Fig. 3.

vertices of the seed triangle, an edge) until it meets another point η on M . The walking of the ball along each edge will define triplets of points that form new triangles till the surface is completely mapped and an interpolating mesh is delineated. During the iterations a condition must always be true: the circumference must be in contact with sample points but the φ -ball must be empty. Translating this abstracted paradigm to a chemical problem we can treat the molecule as the 3D object, its scaffold as the manifold M and the atomic positions as the point-sampling, (Fig. 4 A). It is worth noting that atomic positions out of the bowl (i.e. non-fused substituents) were not appraised because carbon, sulphur and oxygen linkers do not form a continuous surface but rather a graph. It is clear that in computational topology the density of the points cloud is a discriminant parameter for processing a detailed mesh, in spite of the extremely limited number of points analysed (due to the very small list of buckybowl's cartesian coordinates) BPA was able to finely recreate the bowl-shaped features both for sumanene and corannulene skeleton. Compound 2,3,4 and 5 produced a mesh with a very similar triangulation pattern, interpolating 21 vertices and 25 faces. The main difference is related to tetrahedral carbon pinned down on the bowl of compound 2, in fact in this case the central benzenoid ring is not flat (as opposed to compounds 3,4 and 5) but pyramided, the result is a convergence of the lines toward the stereogenic carbon (asterisk in B series, Fig. 4). The exchange of heteroatoms between sumanene and triazasumanene does not alter the triangulation scheme. Focusing on compound 1, the mapped mesh clearly covers a more extended surface with 36 vertices and 39 faces, both corannulene and helical motifs are properly designed.

Curvature analyses

Speaking with the language of differential geometry we can schematize the molecular topologies employing the concept of gaussian curvature, which can be positive, negative or zero. In this situation, the real examples of different types of gaussian curvature are comfortably discussed mentioning the sheet, the bowl and the saddle structures obtained as sp^2 carbon allotrope derivatives (Fig. 5A). Unfortunately, the non-zero curvature molecules (i.e. corannulene, circulene, etc.) are not approximable, except for significant errors, to the notorious spheres, spheroids, and regular saddles for which the curvature is analytically calculated. Physical systems as molecules often display unusual shapes with geometrical irregularities, hence local curvature must be investigated. Applying our attention on buckybowl's in bibliography, the pyramidalization angle (linked to the π -Orbital Axis Vector), the spherical curvature and the bowl-depth are the most used quantities to characterize the local geometry [21–24]. However, despite their direct use in trivalent ordinary systems, they fail for generic geometries, showing limitations and criticalities [25], on the other hand the apparently less intuitive discrete gaussian curvature furnishes an accessible way to scrutinize the local curvature atom by atom. Below the mathematical formalism used in this manuscript.

Let S be a two-dimensional manifold immersed in the 3-dimensional Euclidean space E^3 , the gaussian curvature is the exact value of the integral of K_G over a finite-volume region on a triangulated surface. Applying the Gauss-Bonnet theorem to such a surface, a simple equality,

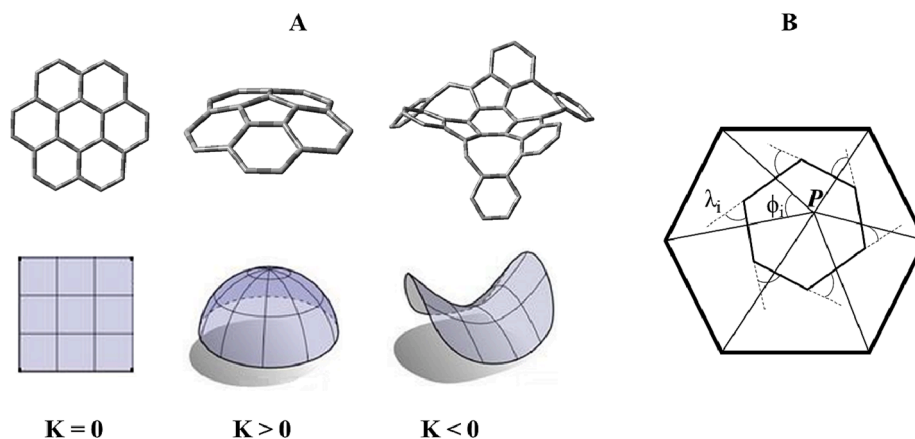


Fig. 5. (A) Schematic sorting of the three different types of gaussian curvature: zero, positive and negative. (B) Angles of a triangulated Voronoi region.

valid over any surface patch, is attained:

$$\iint_S K_G dA = 2\pi - \sum_i \lambda_i \quad (1)$$

where the λ_i are the external angles of the boundary. If we implement this expression to a Voronoi region, the external angle at a circumcenter is simply equal to ϕ_i , the angle of the triangle at the vertex P (Fig. 5 B), therefore:

$$\iint_S K_G dA = 2\pi - \sum_{n=1}^k \phi_i \quad (2)$$

where ϕ_i is the angle of the n -th face at the vertex P_i and k indicates the number of faces around this vertex, the term on the right of the equality is usually called the angle deficit. The last equation defines the local contribution of the gaussian curvature (positive, negative or zero) at P_i , depending on the sign of angle deficit. If we are interested in estimating the local spatial average of the gaussian curvature (also called discrete gaussian curvature) the total gaussian curvature must be divided by the effective area (the area of the faces having P_i as a vertex):

$$A_{eff} = \sum_{P \in k} Area(P) \quad (3)$$

Then the discrete gaussian curvature operator can be expressed as:

$$\bar{K}_G(P_i) = \frac{\iint_S K_G dA}{A_{eff}} \quad (4)$$

DFT functionals benchmark of curvature

When the absorption of circularly polarized light is computationally studied, the CD spectrum fingerprint is strongly dependent on the location of the molecular system within the hypersurface of potential energy[17]. In such terms, in density functional theory, the quality of the simulated structures is heavily affected by the choice of the exchange-correlation functional[26], and it is a commonly accepted practice to benchmark functionals, targeting on the accurate determination of x-ray geometrical parameters such as bonds and angles[27]. However, buckybowls, due to the excessively similar bonds and angles values in their motifs, are not the best candidates for this kind of approach, from this viewpoint a shift of evaluation criterion from the structural parameters to the topological ones is urgent. The atom by atom discrete gaussian curvature reveals a new elegant way to democratize which functional acts better in imitating the curved topology of corannulene and sumanene fragments. In sight of this, a list of functionals (10) was tested to optimize compounds 1–5 (Fig. 3) in gas phase, to cover multiples categories some hybrid, pure and dispersion-

embedded functionals were analyzed. Pople basis set was adopted as it proves to be quite accurate in defining the second-period elements [28,29]. The mean absolute error (MAE) is the chosen parameter in order to evaluate the gaussian curvature goodness between the DFT-calculated and the x-ray data:

$$|\Delta K_{G_{ave}}| = \frac{1}{N} \sum_{i=1}^N |K_{G_{i_{exp}}} - K_{G_{i_{cal}}}| \quad (5)$$

where N is the total number of discrete gaussian curvature values, $K_{G_{i_{exp}}}$ and $K_{G_{i_{cal}}}$ are the i th DFT-calculated and the x-ray computed discrete gaussian curvatures, respectively.

The topological preferences of our test set (Fig. 3.) were verified through the following chronological workflow: 1) optimization process (functional/6-311++G(2d,2p)). 2) BPA surface reconstruction from xyz optimized cartesian coordinates. 3) Computing of the discrete gaussian curvatures.

Fig. 6 and the relative Table 1 give some insights on the accuracy of the DFT functionals to model the discrete gaussian curvature of bowl skeleton atoms, from a first glimpse it can be noted that the presented functionals perform differently for the five corannulene/sumanene cores examined. Indeed, it is not possible to identify a general trend, each compound has its own best performer: compound 1 is excellently described by LC-wPBE, compounds 5 and 2 share their first-rate functional (M06-2X). For the latter compound, B97D dramatically ruins the curvature of buckybowls compared to the other DFT competitors, while for compound 3 and 4 CAM-B3LYP and TPSSSTPSS prevail with their performances. Worth bearing in mind that the high MAEs level for compound 1 (up to about $0.6^\circ/\text{\AA}^2$) could be attributed to the difficult representation of the change of gaussian curvature sign (from positive to negative) passing from the bowl to the helical. It is curious that despite LC-wPBE, M06-2X, CAMB3LYP and TPSSSTPSS were cited about their admirable performances, when the MAEs of the five species are collectively calculated, the APFD crops up as the best functional. By assembling the results obtained from the histograms in Fig. 6 and avoiding any possible bias from single compound evaluation, it appears evident that APFD exquisitely clones the curved topology for all the analyzed compounds.

Once the leader functional was established, it is pivotal to underline that the chiroptical properties and the relative CD spectra are influenced by the solvent effects, on these assumptions an intriguing question spontaneously arrives: Does the solvent environment change the curvature of buckybowls? To answer this query, all the compounds were optimized in their respective spectroscopic reference solvents using the integral equation formalism polarizable continuum model (IEFPCM) at the APFD/6-311++G(2d,2p) level. From Table S1 (supporting information) it is visible that implicit solvent produced a “flatness effect” for

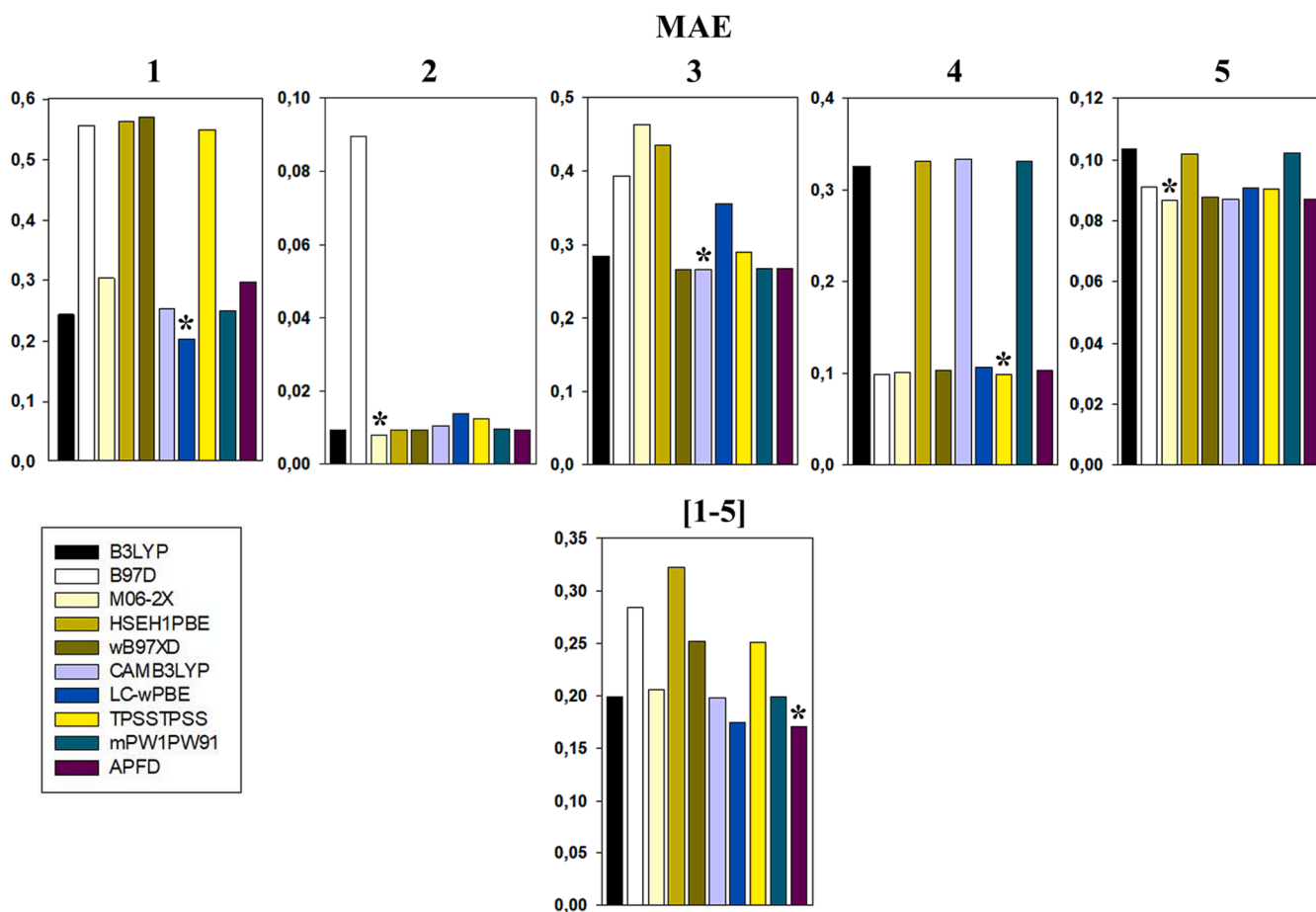


Fig. 6. (Top) Cumulative mean absolute error histograms ($^{\circ}/\text{\AA}^2$) of the discrete gaussian curvatures in gas phase, (Bottom) mean absolute error histograms ($^{\circ}/\text{\AA}^2$) of the whole set in the same condition. Asterisks pinpoint the best performers.

Table 1

Mean absolute errors ($^{\circ}/\text{\AA}^2$) of the discrete gaussian curvature referred to the single compounds and the whole set.

Functional	MAE					
	1	2	3	4	5	[1-5]
B3LYP	0.2413	9.2449e-3	0.2834	0.3265	0.1036	0.1989
B97D	0.5552	0.0895	0.3936	0.0997	0.0912	0.2845
M06-2X	0.3019	7.7961e-3	0.4637	0.1011	0.0868	0.2060
HSEH1PBE	0.5624	9.3221e-3	0.4350	0.3313	0.1019	0.3223
wB97XD	0.5682	9.4087e-3	0.2664	0.1038	0.0878	0.2523
CAMB3LYP	0.2516	0.0104	0.2660	0.3336	0.0872	0.1975
LC-wPBE	0.2025	0.0139	0.3549	0.1072	0.0909	0.1748
TPSSTPSS	0.5487	0.0125	0.2899	0.0992	0.0904	0.2507
mPW1PW91	0.2483	9.7251e-3	0.2666	0.3320	0.1023	0.1988
APFD	0.2960	9.3261e-3	0.2675	0.1034	0.0869	0.1705

all the studied structures, the topological analysis unmistakable shows (both quantitatively and qualitatively) that the total gaussian curvature values are higher in gas phase than in the solvent one. In light of this, it is tangible that in gas phase our selected buckybowls are more curved than in solvent phase. Thinking outside of the structureless continuum implicit model led us to test explicit solvent method to verify if any trend in gaussian curvature is detectable transiting along gas-implicit-explicit pathway. A 25 units solvent box was spherically assembled around each buckyball and the conformational preferences were searched at our target computational level. From the latter results, a decreasing curvature ladder was observed: high curvature (gas), medium curvature (implicit solvent), low curvature (explicit solvent), Fig. 7 (and Table S1). This tendency may be associated to a “relaxation mechanism” of the

Curvature

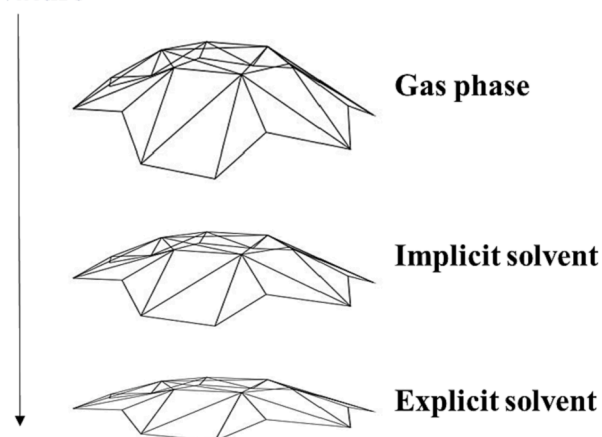


Fig. 7. Decreasing of curvature from gas phase to explicit solvent model. It must be emphasized that, to favor a better visualization of the process, the change of gaussian curvature in the picture was exaggerated.

bowl tension strain, which is blocked in gas phase, but it could be more flexible progressing from implicit to explicit method. This solvent cooperativity is further assisted by functional groups able to establish non-covalent interactions with the explicit solvent sphere (compound 2,4,5).

Circular dichroism spectra simulations by combination of molecular dynamics and TD-DFT

When the chiroptical properties of a chemical system are theoretically inspected, in the most cases the usual procedure is centered on computing ECD *static* spectra (equilibrium structures). As convenient as it is, *static* approach is indifferent to the thermal fluctuations that interest the conformational asymmetry of chiral molecules in solvent phase, as a matter of fact multiple thermal effects contribute to the final spectral signatures and must be considered. All in all, two ingredients shall thus be mixed: 1) an exhaustive phase space conformational sampling of the ground state to get an ensemble of statistically relevant conformations 2) a straightforward methodology to compute, in a cost efficient way, the desired photophysical properties. The use of MD/TD-DFT guarantees the required accuracy to efficiently predict the electric and magnetic dipole moment of the entire system at each time step, the final spectrum will be reconstructed as a weighted sum of the spectra computed at the TD-DFT level on equispaced molecular conformation snapshots extracted from MD simulations. For adherence to point 1 (see above) and to acquire an appropriated description of gaussian curvature over the time (picosecond timescale), ab-initio Born Oppenheimer molecular dynamic simulations in the ground state (implicit solvent phase) were applied to each compound using our dominant functional, APFD. In order to collect the rotatory strengths and the vertical excitation energies indispensable to replicate experimental ECD spectra, APFD, B3LYP, CAM-B3LYP, mPW1PW91 and wB97XD functionals were used. The aforementioned functionals were preferred because, in addition to being tested in the curvature benchmark (section 2.3), are often classified to span the excited-states energy range of chromophoric molecules [30].

At a first glance in Fig. 8. It is possible to see that experimental spectrum of compound 1 can be divided into 3 sections: a positive broad band, a negative shoulder and a negative peak. APFD, mPW1PW91 and B3LYP similarly perform, showing a very detailed spectrum profile with a positive Cotton effect ranging from 309 to 430 nm, slightly red shifted from the experimental one (300–430 nm). The negatively shoulder is finely captured at 295 nm, for these three functionals the negative peak is located between 268 and 275 nm and it represents an excellent

matching with the experimental value (265 nm). On the contrary, CAM-B3LYP and wB97XD display substantial disparities with the recorded spectrum both in terms of band positions and intensities, the final result is an excessively blue shifted effect and a very poor resolution (in both case the negative shoulder is undetectable). Ultimately, APFD is proposed as the best functional performer due to its reliable resolution of negative signatures.

Compound 2 has installed an internal stereogenic carbon on his sumanene hub and reports a very complicated CD spectral pattern. Five positive and negative bands of different wavelength positions and intensities extend from 200 to 500 nm. Again, APFD, mPW1PW91 and B3LYP appear to be pretty satisfactory in emulating the peculiar waving effect of the spectrum (Fig. 9), at lower wavelengths (200–400 nm) the band positions perfectly adhere with the experimental spectrum while in the upper wavelengths regime (400–450 nm) the last large band is moderately red shifted of ~15 nm. The peak magnitudes were respected except for the band at 360 nm and the cusp at 235 nm that are a bit overestimated. CAM-B3LYP and wB97XD, which are practically superimposable, continue to offer insufficient treatment chiefly in the 300–450 nm interval where the band locations are overly blue shifted (about 50 nm). As expected before, APFD still maintains the leadership to recreate the chirality signatures of compound 2.

The C_3 symmetric chiral trimethylsumanene (compound 3) produces a “leveling effect” in the functional performances, indeed all the spectral profiles are decently similar to the real one. Focusing meticulously on Fig. 10. The superb tendency of APFD, mPW1PW91 and B3LYP is able to define a very good fit both for positive peaks and negative valleys. The negative signal at 317 nm is marvelously guessed, while the other three explicit wavelengths are toward-blue placed of about 25 nm (~220, ~240, ~255 nm). In the 200–290 nm region, CAM-B3LYP and wB97XD less suffer of the blue shift effect (~231, ~250, ~264 nm) but marginally mimic the experimental negative spike at 263 nm, which is almost imperceptible (Fig. 10A), an error of 30 nm is recognizable for the upper frequencies signal (~288 nm). For this case, B3LYP was elected the master functional because of its good compromise between intensities ratio and wavelength locations.

Moving from sumanene to triazasumanene the penchant of functionals is retained, in fact the spectral lines of compound 4 are

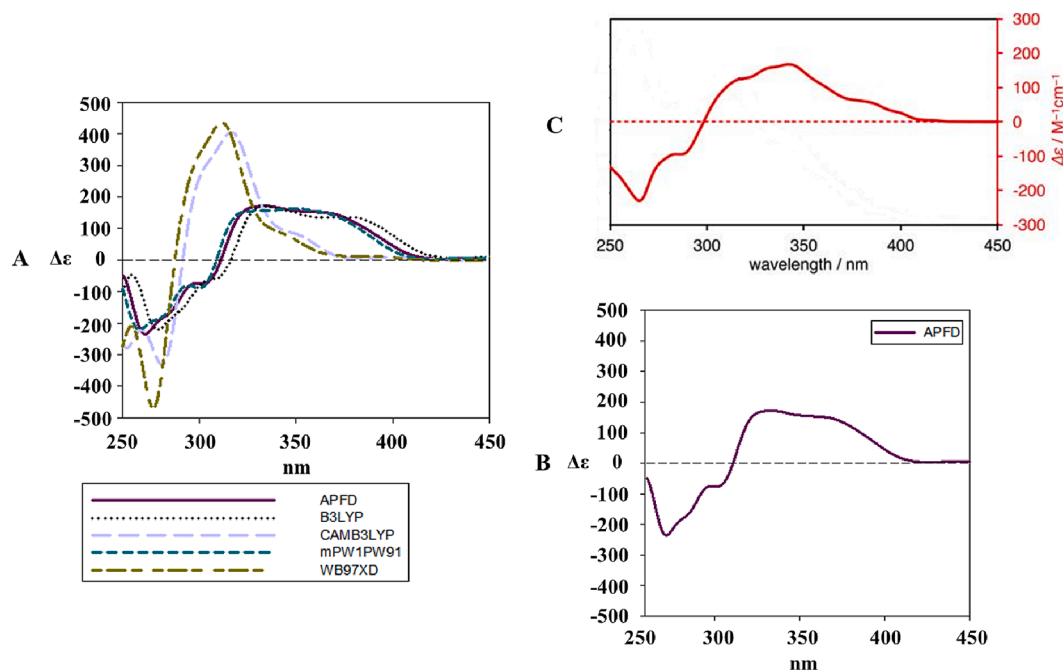


Fig. 8. (A) TD-DFT calculated ECD spectra (functional/6–311++G(2d,2p)) along the MD trajectory for compound 1 in $CHCl_3$. (B) Extraction of the best performer from A (APFD/6–311++G(2d,2p)). (C) Experimental ECD spectrum in chloroform. Adapted from [31]. © 2016 American Chemical Society.

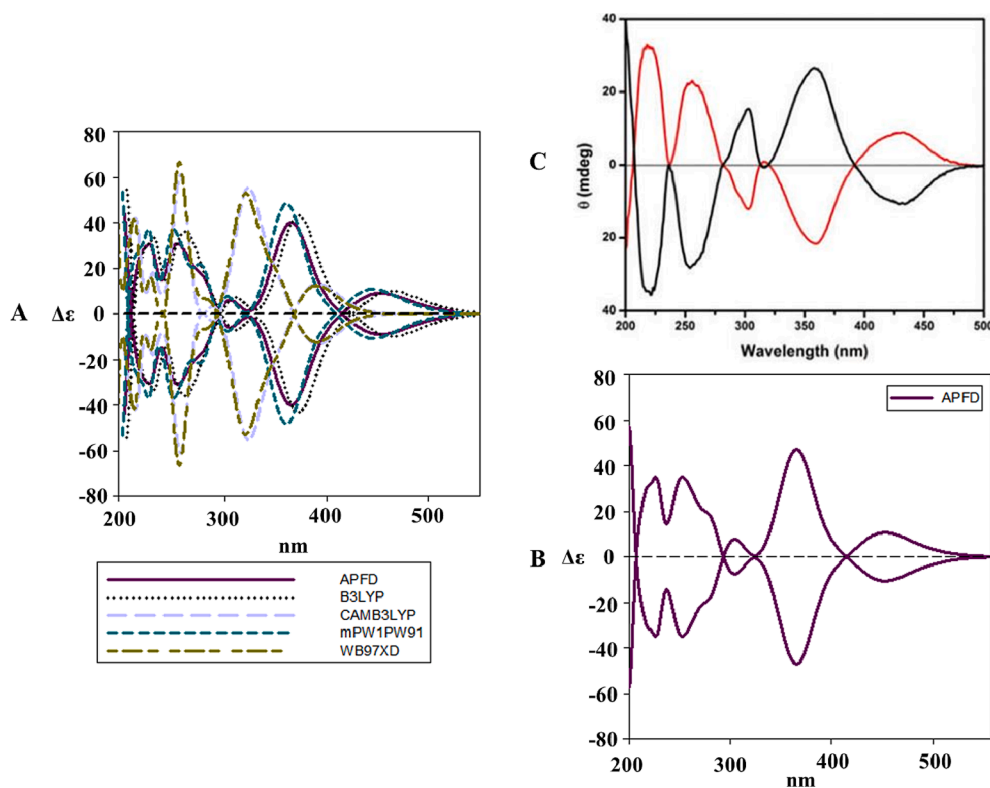


Fig. 9. (A) TD-DFT calculated ECD spectra (functional/6-311++G(2d,2p)) along the MD trajectory for compound 2 in CH_3CN . (B) Extraction of the best performer from A (APFD/6-311++G(2d,2p)). (C) Experimental ECD spectrum in acetonitrile. Adapted from [32] © 2017 Royal Society of Chemistry.

authentically diagrammed by APFD, mPW1PW91 and B3LYP (Fig. 11). As seen for compound 2, the most complex zone is the crest (both positive and negative) at upper wavelengths (372 nm) that is averagely blumoved of 25 nm (345–350 nm). The undulatory behavior composed by the bands at 305 and 275 nm is completely duplicated with high accuracy. Zooming Fig. 11 A emerges that CAM-B3LYP and wB97XD utterly ignore the middle band at 305 nm, showing a *quasi*-silent signal. APFD was approved over all the other functional since it had the ability to grab the little ellipsoid at ~340 nm imputable to the rapid line inversion.

Assuredly, among the systems in Fig. 3. the triaryltriazasumanene (compound 5) has the most challenging circular dichroism spectrum (Fig. 12C), reason why APFD, mPW1PW91, CAM-B3LYP and wB97XD fail to imitate scrupulously the chiral spectral features. The main problem derives from the tricky flat zone around 300 nm that is badly disregarded or substituted with fictitious bands, only B3LYP sufficiently succeeded in replicating the chiral fingerprint both in terms of band shapes and positions. Regrettably, the last signals around 390 nm is almost lost in the base line.

From the previous spectral analysis it is evident that APFD and B3LYP are markedly superior to mPW1PW91, CAM-B3LYP and wB97XD in reproducing ECD spectra of corannulene, sumanene and triazasumanene derivatives. The upper frequency region of the spectra was frequently better described in term of signal position by all the functionals than the lower one. Despite we were strictly interest in the spectral motive, the peak intensities were regularly confirmed in the theoretical model without any excessive over/underestimation of rotational strengths (with the exception of CAM-B3LYP and mPW1PW91 for compound 1, whose helical architecture often impacts on the chiral-sign intensities[36–39]). We further infer that the supremacy of APFD in this section is not random but intimately linked to its capacity in modelling the curvature of different buckybowls (see previous section).

Computational method

All the initial x-ray structures were preliminarily energy-minimized in gas phase using B3LYP, B97D, M06-2X, HSEH1PBE, wB97XD, CAM-B3LYP, LC-wPBE, TPSSSTPSS, mPW1PW91 and APFD coupled with 6-311++G(2d,2p) basis set. APFD/6-311++G(2d,2p) level by means of the IEFPCM method was adopted to evaluate the conformational preferences of the selected buckybowls in the implicit solvent phase, the same computational level was handled to model the explicit solvent phase that was set through a spherically box of solvent around the target molecules (built by Vega ZZ package[40]). Born Oppenheimer Molecular Dynamic (BOMD) simulations were run at 298 K in the ground electronic state (S0) at APFD/6-311++G(2d,2p) level of theory in solvent phase (IEFPCM), with a total time width of 1 ps and a step size of 2 fs. For each compounds, 25 configurations were extracted from the AIMDs (interspersed every 40 fs) and TD-DFT subjected to recover excitation energies, oscillator strengths and rotatory strengths at APFD, B3LYP, CAM-B3LYP, mPW1PW91 and wB97XD/6-311++G(2d,2p) levels, considering the first 50 excited states and assuming the non-equilibrium linear-response (NEQ-LR-PCM) solvent approximation. The ECD intensities $\Delta\epsilon$ were computed as follow[41]:

$$\frac{16\pi^2 N_A R_{0m} E_{abs} \rho(E_{abs})}{3 \cdot 2.303 \cdot \hbar \cdot c} \quad (6)$$

Where N_A is Avogadro's number, \hbar is the reduced Planck's constant, c is the speed of light, $\rho(E_{abs})$ is the gaussian band shape centered in the E_{abs} energy and R_{0m} are the rotational strengths associated to the transition $0 \rightarrow m$. Eq. (5) is expressed in cgs units and the band shape was assumed as gaussian with a bandwidth of 0.25 eV. All the previous calculations were carried out exploiting *Gaussian16* package[42].

The surface reconstructions of buckybowls were executed through Ball Pivoting Algorithm choosing a clustering radius of 20 and an angle threshold of 70° , these geometrical parameters were coherently selected for our specified set of curved molecules. The atom by atom discrete

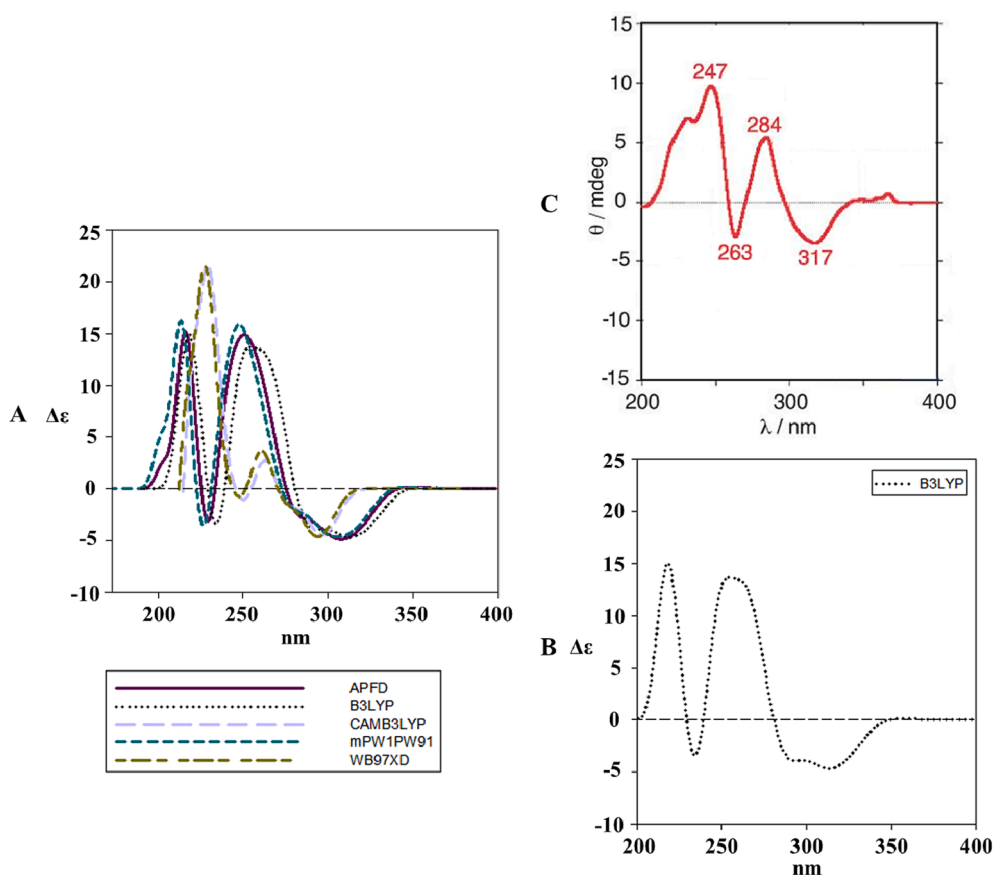


Fig. 10. (A) TD-DFT calculated ECD spectra (functional/6-311++G(2d,2p)) along the MD trajectory for compound 3 in CH_3CN . (B) Extraction of the best performer from A (B3LYP/6-311++G(2d,2p)). (C) Experimental ECD spectrum in acetonitrile. Adapted from [33] © 2012 The Chemical Society of Japan.

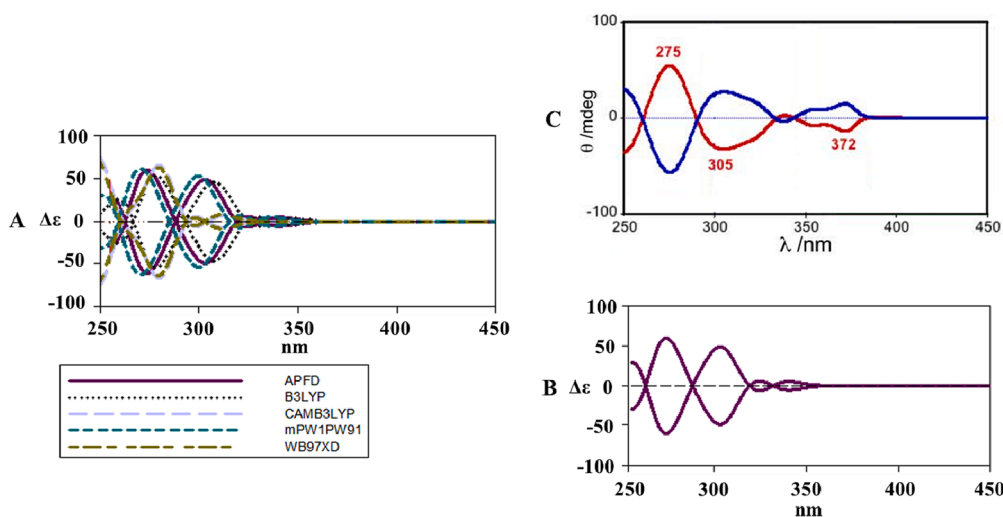


Fig. 11. (A) TD-DFT calculated ECD spectra (functional/6-311++G(2d,2p)) along the MD trajectory for compound 4 in CH_2Cl_2 . (B) Extraction of the best performer from A (APFD/6-311++G(2d,2p)). (C) Experimental ECD spectrum in acetonitrile. Adapted from [34] © 2012 Nature Publishing Group.

gaussian curvatures (xls. files in [supporting information](#)) were obtained from Eq. (4) and visualized thanks to the *Mesh Lab* package[43]. X-ray coordinates were downloaded from the Cambridge Structural Database (CSD) [32–36].

Conclusion

This research performed on a representative set of chiral

buckybowls, made possible to evaluate the importance of topological elements as curvature, aiming to accurately determine both structural and electronic-chiral features of relevance for the circular dichroism spectra calculation of platform-like molecules. Our topological workflow straightforwardly allows to explore the atom by atom discrete gaussian curvature of DFT optimized systems with a very inexpensive post-processing. The presented protocol revealed the following new aspects:

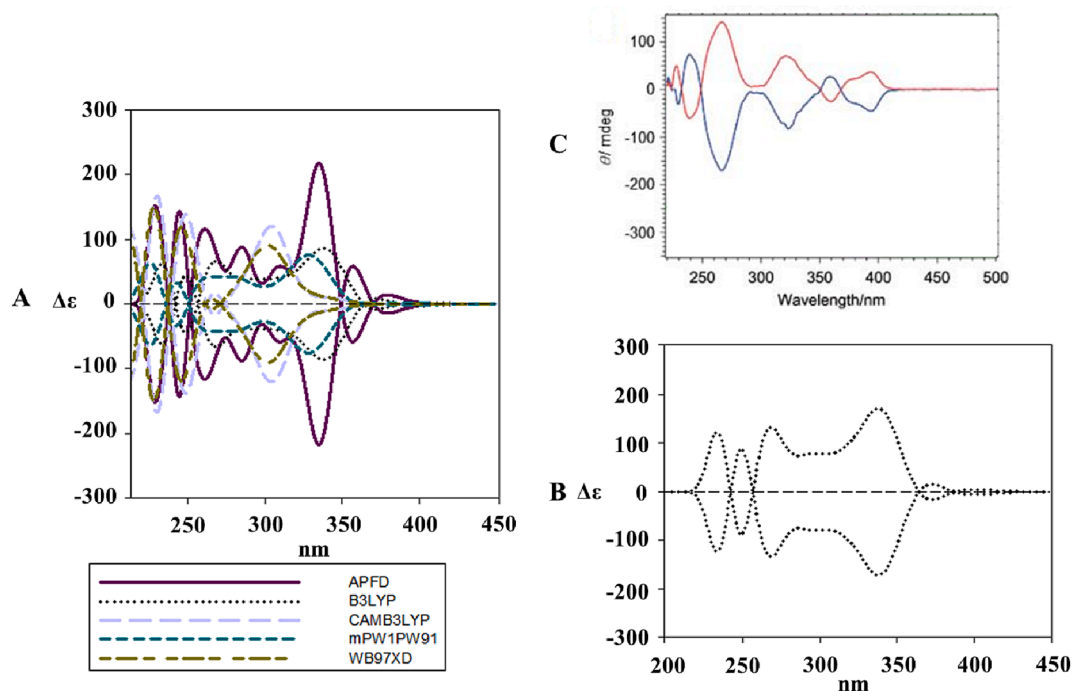


Fig. 12. (A) TD-DFT calculated ECD spectra (functional/6-311++G(2d,2p)) along the MD trajectory for compound 5 in CH_2Cl_2 . (B) Extraction of the best performer from A (B3LYP/6-311++G(2d,2p)). (C) Experimental ECD spectrum in dichloromethane. Adapted from [35] © 2016 The Chemical Society of Japan.

- 1) The Ball Pivoting Algorithm (BPA) demonstrated to be a very useful mathematical tool to rebuild triangulated mesh from the xyz buckybowls cartesian coordinates. In this term BPA was essential to execute a shift of chemical paradigm: from the atomic point cloud to the molecular surface.
- 2) Discrete gaussian curvature operator was applied to every bowl skeleton atom to measure the local curvature, providing a topological quantity to characterize functionalized corannulene and sumanene derivatives.
- 3) Gaussian curvature of buckybowls decreases in the following order: gas phase > implicit solvent model > explicit solvent model.

As result of our DFT functionals benchmark we found that APFD excellently reproduce the buckybowls shape-curvature with a MAE of $0.175^\circ/\text{\AA}^2$ compared to the x-ray data. APFD/6-311++G(2d,2p) computational level was utilized for Born-Oppenheimer molecular dynamic simulations in the implicit solvent phase to determine the thermal-dependent fluctuations by taking into account environmental effects. A list of functionals (APFD, B3LYP, CAM-B3LYP, mPW1PW91, wB97XD) was inspected to analyse the chiro-optical parameters from TD-DFT calculations, the theoretical determined spectra spotlighted that APFD (but also B3LYP is a valid solution) still dominates in elegantly setting the band positions and peak intensities. These findings convince us that our computational plan, optimization/BOMD/TD-DFT based on APFD/6-311++G(2d,2p) level, can act as a useful guide for the *in silico* identification of the most relevant topological properties that govern the observed spectra of chiral buckybowls. We hope our results could motivate experimental synthesis to find new exotic topologies to be studied through the fascinating effect of circularly polarized light.

Declaration of Competing Interest

The authors declare that they have no known competing financial interests or personal relationships that could have appeared to influence the work reported in this paper.

Data availability

Data will be made available on request.

Acknowledgements

The ISCRA (CINECA) supercomputing initiative is acknowledged for computational time provided.

Appendix A. Supplementary data

Supplementary data to this article can be found online at <https://doi.org/10.1016/j.flatc.2023.100509>.

References

- [1] Y. Segawa, H. Ito, K. Itami, Structurally uniform and atomically precise carbon nanostructures, *Nat. Rev. Mater.* 1 (2016) 15002.
- [2] V. Georgakilas, J.A. Perman, J. Tucek, R. Zboril, Broad Family of Carbon Nanoallotropes: Classification, Chemistry, and Applications of Fullerenes, Carbon Dots, Nanotubes, Graphene, Nanodiamonds, and Combined Superstructures, *Chem. Rev.* 115 (2015) 4744–4822.
- [3] Z. Li, Z. Liu, H. Sun, C. Gao, Superstructured Assembly of Nanocarbons: Fullerenes, Nanotubes, and Graphene, *Chem. Rev.* 115 (2015) 7046–7117.
- [4] X. Li, F. Kang, M. Inagaki, Buckybowls: Corannulene and Its Derivatives, *Small* 12 (2016) 3206–3223.
- [5] T.A.A. Broadbent, *Excursions into Mathematics*. By A. Beck, M. N. Bleicher and D. W. Crowe. Pp. xxi, 489. 1969. (Worth Publishers, Inc., New York.), *Math. Gaz.* 54. (1970). 167–168.
- [6] M. Rickhaus, M. Mayor, M. Jurček, Chirality in curved polyaromatic systems, *Chem. Soc. Rev.* 46 (2017) 1643–1660.
- [7] Y. Wang, O. Allemann, T.S. Balaban, N. Vanthuyne, A. Linden, K.K. Baldrige, J. S. Siegel, Chiral Atropisomeric Indenocorannulene Bowls: Critique of the Cahn–Ingold–Prelog Conception of Molecular Chirality, *Angew. Chem. Int. Ed.* 57 (2018) 6470–6474.
- [8] S. Higashibayashi, Chapter 4 - Control of Inversion Kinetics of Bowl-Shaped Aromatic Compounds, in: M. Numata, S. Yagai, T. Hamura (Eds.), *Kinetic Control in Synthesis and Self-Assembly*, Academic Press, 2019, pp. 65–96.
- [9] S. Higashibayashi, H. Sakurai, Asymmetric synthesis of a chiral bucky bowl, trimethylsumanene, *J. Am. Chem. Soc.* 130 (2008) 8592–8593.
- [10] T. Ryoji, H. Shuhei, I. Takeharu, T. Shinji, S. Hidehiro, Optical Resolution of Chiral Buckybowls by Chiral HPLC, *Chem. Lett.* 39 (2010) 646–647.

- [11] Q. Tan, P. Kaewmati, S. Higashibayashi, M. Kawano, Y. Yakiyama, H. Sakurai, Triazasumanene: An Isoelectronic Heteroanalogue of Sumanene, *Bull. Chem. Soc. Jpn.* 91 (4) (2018) 531–537.
- [12] K. Kanagaraj, K. Lin, W. Wu, G. Gao, Z. Zhong, D. Su, C. Yang, Chiral Buckybowl Molecules, *Symmetry* 9 (2017) 174.
- [13] S. Liu, Z. Sun, M. Liang, W. Song, R. Zhang, Y. Shi, Y. Cui, Q. Gao, An Unrevealed Molecular Function of Corannulene Buckybowl Glycoconjugates in Selective Tumor Annihilation by Targeting the Cancer-Specific Warburg Effect, *Adv. Sci.* 9 (2022) 2105315.
- [14] X. Tian, L.M. Roch, N. Vanthuyne, J. Xu, K.K. Baldrige, J.S. Siegel, Azaindenocorannulenes: Synthesis, Properties, and Chirality, *Org. Lett.* 21 (2019) 3510–3513.
- [15] G. Bella, M. Milone, G. Bruno, A. Santoro, Which DFT factors influence the accuracy of ¹H, ¹³C and ¹⁹⁵Pt NMR chemical shift predictions in organopolymetallic square-planar complexes? New scaling parameters for homo- and hetero-multimetallic compounds and their direct applications, *Phys. Chem. Chem. Phys.* 24 (2022) 26642–26658.
- [16] G. Bella, A. Rotondo, Theoretical prediction of ¹³C NMR spectrum of mixed triglycerides by mean of GIAO calculations to improve vegetable oils analysis, *Chem. Phys. Lipids* 232 (2020) 104973.
- [17] Y. Nakai, T. Mori, Y. Inoue, Theoretical and experimental studies on circular dichroism of carbo[n]helicenes, *J. Phys. Chem. A* 116 (27) (2012) 7372–7385.
- [18] J. Mack, Y. Morita, S. Higashibayashi, H. Sakurai, N. Kobayashi, Magnetic circular dichroism spectroscopy and electronic structures of C₃ symmetry buckybowl, *Chem. Phys. Lett.* 556 (2013) 188–194.
- [19] R.G. Woolley, Must a molecule have a shape? *J. Am. Chem. Soc.* 100 (4) (1978) 1073–1078.
- [20] F. Bernardini, J. Mittleman, H. Rushmeier, C. Silva, G. Taubin, The ball-pivoting algorithm for surface reconstruction, *IEEE Trans. Vis. Comput. Graph.* 5 (4) (1999) 349–359.
- [21] R.C. Haddon, Hybridization and the orientation and alignment of pi-orbitals in nonplanar conjugated organic molecules: pi-orbital axis vector analysis (POAV2), *J. Am. Chem. Soc.* 108 (1986) 2837–2842.
- [22] R.C. Haddon, C₆₀: Sphere or Polyhedron? *J. Am. Chem. Soc.* 119 (1997) 1797–1798.
- [23] R.C. Haddon, L.T. Scott, π -Orbital conjugation and rehybridization in bridged annulenes and deformed molecules in general: π -orbital axis vector analysis, *Pure Appl. Chem.* 58 (1986) 137–142.
- [24] B.B. Shrestha, S. Karanjit, S. Higashibayashi, H. Sakurai, Correlation between bowl-inversion energy and bowl depth in substituted sumanenes, *Pure Appl. Chem.* 86 (2014) 747–753.
- [25] J. Sabalot-Cuzzubbo, G. Salvato-Vallverdu, D. Bégué, J. Cresson, Relating the molecular topology and local geometry: Haddon's pyramidalization angle and the Gaussian curvature, *J. Chem. Phys.* 152 (2020), 244310.
- [26] G. Bella, A. Santoro, F. Nicolò, G. Bruno, M. Cordaro, Do Secondary Electrostatic Interactions Influence Multiple Dihydrogen Bonds? AA–DD Array on an Amine-Borane Aza-Coronand, *Theoretical Studies and Synthesis* 22 (2021) 593–605.
- [27] É. Brémond, M. Savarese, N.Q. Su, Á.J. Pérez-Jiménez, X. Xu, J.C. Sancho-García, C. Adamo, Benchmarking Density Functionals on Structural Parameters of Small-/Medium-Sized Organic Molecules, *J. Chem. Theory Comput.* 12 (2016) 459–465.
- [28] G. Bella, A. Santoro, M. Cordaro, F. Nicolò, G. Bruno, Isoxazolone Reactivity Explained by Computed Electronic Structure Analysis, *Chin. J. Chem.* 38 (2020) 163–168.
- [29] B.C. Ferrari, C.J. Bennett, A Comparison of Medium-Sized Basis Sets for the Prediction of Geometries, Vibrational Frequencies, Infrared Intensities and Raman Activities for Water, *J. Phys. Conf. Ser.* 1290 (2019), 012013.
- [30] A.M. Grabarz, B. Ośmiałowski, Benchmarking Density Functional Approximations for Excited-State Properties of Fluorescent Dyes, *Molecules* 26 (2021) 7434.
- [31] T. Fujikawa, D.V. Preda, Y. Segawa, K. Itami, L.T. Scott, Corannulene-Helicene Hybrids: Chiral π -Systems Comprising Both Bowl and Helical Motifs, *Org. Lett.* 18 (2016) 3992–3995.
- [32] N. Ngamsomprasert, J.-S. Dang, S. Higashibayashi, Y. Yakiyama, H. Sakurai, Sumanene derivatives functionalized at the internal carbon, *Chem. Comm.* 53 (2017) 697–700.
- [33] S. Higashibayashi, R. Tsuruoka, Y. Soujanya, U. Purushotham, G.N. Sastry, S. Seki, T. Ishikawa, S. Toyota, H. Sakurai, Trimethylsumanene: Enantioselective Synthesis, Substituent Effect on Bowl Structure, Inversion Energy, and Electron Conductivity, *Bull. Chem. Soc. Jpn.* 85 (2012) 450–467.
- [34] Q. Tan, S. Higashibayashi, S. Karanjit, H. Sakurai, Enantioselective synthesis of a chiral nitrogen-doped buckybowl, *Nat. Comm.* 3 (2012) 891.
- [35] P. Kaewmati, Q. Tan, S. Higashibayashi, Y. Yakiyama, H. Sakurai, Synthesis of Triaryltriazasumanenes, *Chem. Lett.* 46 (2017) 146–148.
- [36] N.J. Schuster, L.A. Joyce, D.W. Paley, F. Ng, M.L. Steigerwald, C. Nuckolls, The Structural Origins of Intense Circular Dichroism in a Wagging Helicene Nanoribbon, *J. Am. Chem. Soc.* 142 (2020) 7066–7074.
- [37] X. Xiao, S.K. Pedersen, D. Aranda, J. Yang, R.A. Wiscons, M. Pittelkow, M. L. Steigerwald, F. Santoro, N.J. Schuster, C. Nuckolls, Chirality Amplified: Long, Discrete Helicene Nanoribbons, *J. Am. Chem. Soc.* 143 (2) (2021) 983–991.
- [38] Y. Nakai, T. Mori, Y. Inoue, Circular Dichroism of (Di)methyl- and Diaza[6] helicenes. A Combined Theoretical and Experimental Study, *J. Phys. Chem. A* 117 (2013) 83–93.
- [39] J. Roose, S. Achermann, O. Dumele, F. Diederich, Electronically Connected [n] Helicenes: Synthesis and Chiroptical Properties of Enantiomerically Pure (E)-1,2-Di ([6]helicene-2-yl)ethenes, *Eur. J. Org. Chem.* 2013 (2013) 3223–3231.
- [40] A. Pedretti, L. Villa, G. Vistoli, VEGA: a versatile program to convert, handle and visualize molecular structure on Windows-based PCs, *Journal of molecular graphics & modelling* 21 (2002) 47–49.
- [41] G. Longhi, E. Castiglioni, S. Abbate, F. Lebon, D.A. Lightner, Experimental and Calculated CPL Spectra and Related Spectroscopic Data of Camphor and Other Simple Chiral Bicyclic Ketones, *Chirality* 25 (2013) 589–599.
- [42] M.J. Frisch, G.W. Trucks, H.B. Schlegel, G.E. Scuseria, M.A. Robb, J.R. Cheeseman, G. Scalmani, V. Barone, G.A. Petersson, H. Nakatsuji, X. Li, M. Caricato, A.V. Marenich, J. Bloino, B.G. Janesko, R. Gomperts, B. Mennucci, H.P. Hratchian, J.V. Ortiz, A.F. Izmaylov, J.L. Sonnenberg, Williams, F. Ding, F. Lipparini, F. Egidi, J. Goings, B. Peng, A. Petrone, T. Henderson, D. Ranasinghe, V.G. Zakrzewski, J. Gao, N. Rega, G. Zheng, W. Liang, M. Hada, M. Ehara, K. Toyota, R. Fukuda, J. Hasegawa, M. Ishida, T. Nakajima, Y. Honda, O. Kitao, H. Nakai, T. Vreven, K. Throssell, J.A. Montgomery Jr., J.E. Peralta, F. Ogliaro, M.J. Bearpark, J.J. Heyd, E.N. Brothers, K.N. Kudin, V.N. Staroverov, T.A. Keith, R. Kobayashi, J. Normand, K. Raghavachari, A.P. Rendell, J.C. Burant, S.S. Iyengar, J. Tomasi, M. Cossi, J.M. Millam, M. Klene, C. Adamo, R. Cammi, J.W. Ochterski, R.L. Martin, K. Morokuma, O. Farkas, J.B. Foresman, D.J. Fox, *Gaussian 16 Rev. C.01*, in, Wallingford, CT, 2016.
- [43] P. Cignoni, M. Callieri, M. Corsini, M. Dellepiane, F. Ganovelli, G. Ranzuglia, MeshLab: an Open-Source Mesh Processing Tool, in (2008) 129–136.